Low-energy $M1$ excitations in ^{208}Pb and the spin channel of the Skyrme energy-density functional

V. Tselyaev,[1,*] N. Lyutorovich,[1] J. Speth,[2] P.-G. Reinhard,[3] and D. Smirnov[1]

[1]*St. Petersburg State University, St. Petersburg 199034, Russia*

[2]*Institut für Kernphysik, Forschungszentrum Jülich, D-52425 Jülich, Germany*

[3]*Institut für Theoretische Physik II, Universität Erlangen-Nürnberg, D-91058 Erlangen, Germany*

(Received 6 March 2019; published 26 June 2019)

We investigate the performance of the Skyrme energy-density functional with respect to magnetic modes, checking in particular the impact of the spin-orbit and spin-spin interaction. Test cases are the low-energy $M1$ excitations in ^{208}Pb treated within the self-consistent random-phase approximation based on the Skyrme energy-density functional. We scan a large variety of Skyrme parametrizations to find out which parameters of the functional have strongest correlations with $M1$ properties. We explore a simple method of the modification of the spin-related parameters, which delivers a better description of $M1$ excitations while basically maintaining the good description of ground-state properties.

DOI: 10.1103/PhysRevC.99.064329

I. INTRODUCTION

The aim of this paper is to explore the self-consistent description of nuclear magnetic excitations by an energy-density functional (EDF) of Skyrme type [1] taking the low-lying magnetic dipole ($M1$) excitations in ^{208}Pb as test case. Tool of choice is the random phase approximation (RPA) and its various extensions which is the most often used method for the investigation of nuclear excitation spectra. It takes as input data single-particle (sp) energies, sp wave functions and a particle-hole (ph) residual interaction. Early calculations as, e.g., Migdal's theory of finite Fermi systems (TFFS, see Refs. [2–4]) started with an effective single-particle model whose parameters are adjusted to experimental sp properties and used (in nearly all numerical applications) a density-dependent zero-range ph interaction. It requires only a few parameters, coined Landau-Migdal (LM) parameters, which are adjusted to electric and magnetic nuclear excitations and which turn out to be universal in the sense that the same values apply throughout the chart of nuclei [5]. In self-consistent nuclear models, one obtains the sp properties as well as the ph interaction from one and the same effective Hamiltonian, or EDF respectively. The parameters of the Skyrme EDF are primarily adjusted to bulk properties of the nuclear ground state. An appropriate ph residual interaction is not a priori guaranteed. For example, the first realistic Skyrme parametrizations [6,7] had an incompressibility of the order of 350 MeV and produced therefore the breathing mode in ^{208}Pb at around 17 MeV (which was off by 3 MeV from the experimental value measured some years later). Including data specific to excitations, one could later on develop parametrizations which also perform well for breathing mode and isoscalar quadrupole resonance [8,9]. In general, there is sufficient flexibility in the Skyrme EDF to accommodate all modes with natural parity, isoscalar as well as isovector resonances [10]. The LM parameters for natural-parity excitations derived from such Skyrme EDFs agree nicely with long tested LM parameters of TFFS [11].

For magnetic modes, self-consistent models as, e.g., Skyrme EDFs have not yet reached that high level of descriptive power while TFFS has been adapted very well also for these excitation channels. The plan for this paper is thus to explore the chances for a better description of magnetic modes with a Skyrme EDF exploiting yet loosely determined aspects of the functional. Here we are guided by the large body of experience gathered within the TFFS. It tells us that the spin dependent ph interaction is weak for the isoscalar part and is strongly repulsive for the isovector part. This agrees with the experimental findings: There are no isoscalar collective magnetic resonances over the whole periodic system but there exist strong Gamow-Teller resonances in heavy nuclei, which are created by the spin-isospin-dependent part of the residual interaction. We also know from such investigations that the $M1$ states in ^{208}Pb represent an ideal test case. Experimental data on the distribution of the $M1$ strength in this nucleus at the excitation energies up to 8.4 MeV are known since the work of Refs. [12–14]. Updates for the energies below neutron separation energy were published in Ref. [15]. The observed spectrum of the low-energy $M1$ excitations in ^{208}Pb consists of two marked features: an isoscalar 1^+ state with $E = 5.844$ MeV and a broad isovector $M1$ resonance in the interval 6.6–8.1 MeV. Strong fragmentation of the $M1$ resonance was one of the reasons for the difficulties with identification in the early experiments (see, e.g., Ref. [16] for discussion). Moreover, several states that had been originally identified as $M1$ turned out to be $E1$ after experiments with polarized photons were available.

The numerous theoretical papers devoted to the microscopic description of $M1$ excitations in ^{208}Pb can be divided into two main groups. The first group includes the papers in which the nuclear excitations are treated as superposition

*tselyaev@mail.ru

of the one-particle–one-hole (1ph) configurations, i.e. within the RPA or the Tamm-Dancoff approximation (see, in particular, Refs. [3,4,17–24]). In the papers of the second group, various versions of beyond-RPA approaches are used in which the RPA configuration space is enlarged by adding the 2ph, 1ph $\otimes$ phonon or two-phonons configurations (see, e.g., Refs. [25–31]). Most of the earlier work as mentioned before was performed within the TFFS. Using experimental single-particle energies as input for the mean-field part and properly tuning the interaction parameters (LM parameters) in the spin-spin channel, they managed to provide an appropriate description of peaks and $M1$ strengths. Beyond-RPA treatments, properly including the coupling of 1ph states to 2ph configurations, were necessary to describe the spectral fragmentation of the $M1$ resonance around 7.5 MeV [31].

Fully self-consistent RPA calculations as done in Refs. [20–24] did not yet reach that level of description. In fact, there is no published Skyrme parametrization that can describe simultaneously position and strength of $M1$ modes in ^{208}Pb and other nuclei [21,22]. Already ^{208}Pb alone seems to pose insurmountable difficulties. It is hard to get the lower $M1$ peak and the $M1$ resonance simultaneously at their correct energies, not to mention a proper prediction of $M1$ strength. Inappropriate strengths of spin-orbit coupling were identified as one major source of the problem [21,22]. We had applied a recently optimized phonon-coupling model on top of self-consistent RPA [32,33] to $M1$ modes and, unfortunately, did not find any improvement concerning spectral separation of lower and upper mode nor sufficiently strong fragmentation. The problem has first to be cleared at RPA level before invoking more advanced approaches.

In our paper we address two major tasks. In the first part we present a thorough overview of the performance of many published Skyrme forces concerning their spin stability and the $M1$ modes. In a second step, we exploit the experience gathered in the first part to move toward a Skyrme parametrization for fully self-consistent calculations, which describe characteristics of the leading $M1$ modes correctly. To this end we determine the crucial handles in the Skyrme energy functionals, which have the most impact on the $M1$ spectrum. They include two groups of the parameters being the coupling constants of the spin-spin and the spin-orbit terms of the Skyrme EDF. The first group is closely related to the spin-spin parameters of the residual interaction used in the TFFS. The parameters of the second group govern the spin-orbit splitting of the single-particle states and were examined in this context by many authors including Skyrme himself (see Refs. [34,35]). The problem that we try to solve in the present paper is to tune all these parameters to deliver correct energies and strengths of the leading $M1$ modes in ^{208}Pb within the fully self-consistent RPA based on the Skyrme EDF without spoiling the high quality with respect to nuclear ground-state observables achieved in the original parametrizations of this functional.

The paper is organized as follows. Section II provides the formal background of RPA, the Skyrme functional, the magnetic operators, and the numerical scheme. Section III discusses $M1$ modes in the context of Skyrme EDFs and works out the leading mechanisms defining these modes. In Sec. IV we try a moderate readjustment of Skyrme parameters, which leads to better description of $M1$ modes. The last section contains the conclusions.

II. FORMAL BACKGROUND

A. Summary of the RPA

Within the RPA one can calculate the spectrum of the excitation energies ω_n of the even-even nucleus and the corresponding set of the transition amplitudes Z^n_{12} where the numerical indices $(1, 2, 3, \ldots)$ stand for the sets of the quantum numbers of some single-particle basis. Generally, this basis can be arbitrary, but it is convenient to suppose that it diagonalizes the single-particle density matrix ρ_{12} and the single-particle Hamiltonian h_{12}, which satisfy the relations $\rho^2 = \rho$ and $[\,h, \rho\,] = 0$. In this case the following equations are fulfilled:

$$h_{12} = \varepsilon_1 \delta_{12}, \quad \rho_{12} = n_1 \delta_{12}. \tag{1}$$

In what follows the indices p and h will be used to label the single-particle states of the particles ($n_p = 0$) and holes ($n_h = 1$) in this basis.

The RPA eigenvalue equation has the form

$$\sum_{34} \Omega^{\rm RPA}_{12,34}\, Z^n_{34} = \omega_n\, Z^n_{12}, \tag{2}$$

where

$$\Omega^{\rm RPA}_{12,34} = h_{13}\,\delta_{42} - \delta_{13}\,h_{42} + \sum_{56} M^{\rm RPA}_{12,56}\, V_{56,34}, \tag{3}$$

$$M^{\rm RPA}_{12,34} = \delta_{13}\,\rho_{42} - \rho_{13}\,\delta_{42}, \tag{4}$$

V is the amplitude of the residual interaction and $M^{\rm RPA}$ is the metric matrix. The matrices $\Omega^{\rm RPA}$ and $M^{\rm RPA}$ act in the ph + hp space. The transition amplitudes Z^n_{12} are normalized to

$$\sum_{1234} Z^{n*}_{12}\, M^{\rm RPA}_{12,34}\, Z^{n'}_{34} = {\rm sgn}(\omega_n)\,\delta_{n,\,n'}. \tag{5}$$

In the self-consistent RPA, which is supposed in the following, the following relations are fulfilled:

$$h_{12} = \frac{\delta E[\rho]}{\delta \rho_{21}}, \quad V_{12,34} = \frac{\delta^2 E[\rho]}{\delta \rho_{21}\,\delta \rho_{34}}, \tag{6}$$

where $E[\rho]$ is an energy-density functional.

The amplitudes Z^n_{12} allow us to calculate the reduced probabilities of the transitions caused by the external field operator Q^α_{LM} according to the formula

$$B_n(\alpha L_n) = \sum_{M_n} \left|\left\langle Z^n \,\middle|\, Q^\alpha_{L_n M_n}\right\rangle\right|^2, \tag{7}$$

where index α labels different kinds of the operators of the multipolarity L (in particular, $\alpha = m$ for the magnetic transitions).

B. Skyrme energy-density functional

As the energy-density functional $E[\rho]$ in Eqs. (6) we take the Skyrme EDF of the standard form (see, e.g.,

Refs. [36,37]). It can be represented as the sum of the following terms:

$$E_{\rm Skyrme} = E_{\rm kin} + E_{\rm int} + E_{\rm Coul}, \tag{8}$$

where

$$E_{\rm kin} = \int d\boldsymbol{r}\left[\frac{\hbar^2}{2m_p}\tau_p(\boldsymbol{r}) + \frac{\hbar^2}{2m_n}\tau_n(\boldsymbol{r})\right], \tag{9}$$

$$E_{\rm int} = \int d\boldsymbol{r}\,\mathcal{E}_{\rm int}(\boldsymbol{r}), \tag{10}$$

$$E_{\rm Coul} = \frac{e^2}{2}\int d\boldsymbol{r}\,d\boldsymbol{r}'\,\frac{\rho_p(\boldsymbol{r})\rho_p(\boldsymbol{r}')}{|\boldsymbol{r}-\boldsymbol{r}'|} - \frac{3e^2}{4}\left(\frac{3}{\pi}\right)^{1/3}\int d\boldsymbol{r}\,\rho_p^{4/3}(\boldsymbol{r}). \tag{11}$$

The energy density in Eq. (10) is given by

$$\begin{aligned}\mathcal{E}_{\rm int} = \sum_{T=0,1}\big[&C_T^{\rho}\,\rho_T^2 + C_T^{\rho,\alpha}\,\rho_T^2\rho_0^{\alpha} + C_T^{\Delta\rho}\,\rho_T\Delta\rho_T \\ &+ C_T^{\tau}\left(\rho_T\tau_T - \boldsymbol{j}_T^2\right) + C_T^{J}\left(\boldsymbol{J}_T^2 - \boldsymbol{s}_T\cdot\boldsymbol{T}_T\right) \\ &+ C_T^{\nabla J}\left(\rho_T\nabla\cdot\boldsymbol{J}_T + \boldsymbol{s}_T\cdot\nabla\times\boldsymbol{j}_T\right) \\ &+ C_T^{s}\,\boldsymbol{s}_T^2 + C_T^{s,\alpha}\,\boldsymbol{s}_T^2\rho_0^{\alpha} + C_T^{\Delta s}\,\boldsymbol{s}_T\Delta\boldsymbol{s}_T\big],\end{aligned} \tag{12}$$

where C_T^{ρ}, $C_T^{\rho,\alpha}$, $C_T^{\Delta\rho}$, C_T^{τ}, C_T^{J}, $C_T^{\nabla J}$, C_T^{s}, $C_T^{s,\alpha}$, $C_T^{\Delta s}$, and α are the constants, ρ_T, τ_T, $\boldsymbol{J}_T$, $\boldsymbol{s}_T$, $\boldsymbol{T}_T$, and $\boldsymbol{j}_T$ are the local densities and currents. These densities and currents are divided into two groups (see Refs. [1,38]): time-even (ρ_T, τ_T, $\boldsymbol{J}_T$) and time-odd ($\boldsymbol{s}_T$, $\boldsymbol{T}_T$, $\boldsymbol{j}_T$). Their definition through the single-particle density matrix is given in Appendix A.

In the general case, if the form of the functional $E_{\rm int}$ is constrained only by the conditions of the global symmetries, the C constants are the independent parameters. Usually, they are determined by fitting the results of the Skyrme-Hartree-Fock (SHF) and RPA calculations to the experimental data on basic nuclear properties with taking into account the constraints imposed by the nuclear matter properties. However, if the Skyrme EDF, Eqs. (8)–(12), is derived within the Hartree-Fock approximation from the many-body Hamiltonian containing two-body velocity- and density-dependent zero-range interaction, the number of the independent C constants decreases. In this case 18 C constants in Eq. (12) are expressed through 10 Skyrme-force parameters t_0, x_0, t_1, x_1, t_2, x_2, t_3, x_3, W_0, and x_W (see, e.g., Ref. [1]). The respective formulas are given in Appendix B.

Different bias in choosing the data and steady growth of information on exotic nuclei has led to a great variety of parametrizations. In order to keep the present survey sufficiently general, we consider a large set of 30 different parametrizations of the Skyrme EDF: SIII [7], SGII [39], SkM* [8,9], RATP [40], T5 and T6 [41], SkP [42], SkI3, SkI4, and SkI5 [43], SLy4, SLy5, and SLy6 [44], SKX, SKXm, and SKXce [45], SkO and SkO′ [46], MSk1 and MSk3 [47], MSk9 [48], SV-bas, SV-K218, SV-kap00, SV-mas07, SV-sym34, and SV-min [10], SV-m56k6 and SV-m64k6 [49], and SAMi [50].

Here it should be noted that the time-odd densities and currents are equal to zero in the ground states of the even-even nuclei [38]. So, the constants C_T^{s}, $C_T^{s,\alpha}$, and $C_T^{\Delta s}$ do not affect the ground-state properties of these nuclei and the mean field deduced by making use of Eq. (6). Nevertheless, these constants can have an impact on the characteristics of the excited states of the even-even nuclei because in the general case the respective terms of the functional $E_{\rm int}$ give the nonzero contribution to the residual interaction according to Eqs. (6), (8), (10), and (12), even if the time-odd densities and currents are equal to zero. This circumstance allows us to change the constants C_T^{s}, $C_T^{s,\alpha}$, and $C_T^{\Delta s}$ (assuming that they are the independent parameters) for the purpose of description of nuclear excitations without affecting the ground state and the self-consistent mean field.

It is known that the parameters C_T^{s}, $C_T^{s,\alpha}$, and $C_T^{\Delta s}$ in most cases have little influence on the characteristics of the natural parity excitations, but in some cases can lead to the spin instability in the self-consistent RPA and extended RPA calculations. In particular for this reason sometimes (including our recent papers [32,33,51–53]) they are set to be equal to zero, while the other C constants are determined by the Skyrme-force parameters according to Eqs. (B1). However, this choice is not suitable for the self-consistent description of the magnetic excitations which are the subject of the present paper. In this case the terms of the functional $E_{\rm int}$ containing the constants C_T^{s}, $C_T^{s,\alpha}$, and $C_T^{\Delta s}$ become relevant. In particular, from Eqs. (6), (8), (10), and (12) it follows that the terms containing C_T^{s} yield the term V^s of the residual interaction V having the form of the Landau-Migdal ansatz

$$V^s = C_N\left(g\,\boldsymbol{\sigma}\cdot\boldsymbol{\sigma}' + g'\,\boldsymbol{\sigma}\cdot\boldsymbol{\sigma}'\,\boldsymbol{\tau}\cdot\boldsymbol{\tau}'\right), \tag{13}$$

where

$$C_{\rm N}\,g = 2\,C_0^{s}, \quad C_{\rm N}\,g' = 2\,C_1^{s}, \tag{14}$$

$C_{\rm N}$ is a normalization constant. Just the parameters g and g' in Eq. (13) are responsible for the description of the unnatural parity excitations in the TFFS (see Refs. [2–4]). The method of determining the C constants of the functional $E_{\rm int}$ adopted in the present paper is described in Sec. IV.

C. $M1$ operator

The field operator Q in the case of the $M1$ excitations has the following (vector) form:

$$\boldsymbol{Q} = \mu_N\sqrt{\frac{3}{16\pi}}\{(\gamma_n+\gamma_p)\,\boldsymbol{\sigma} + \boldsymbol{l} + [(1-2\xi_s)(\gamma_n-\gamma_p)\,\boldsymbol{\sigma} - (1-2\xi_l)\,\boldsymbol{l}]\,\tau_3\}, \tag{15}$$

where $\boldsymbol{l}$ is the single-particle operator of the angular momentum, $\boldsymbol{\sigma}$ and τ_3 are the spin and isospin Pauli matrices, respectively (with positive eigenvalue of τ_3 for the neutrons), $\mu_N = e\hbar/2m_pc$ is the nuclear magneton, $\gamma_p = 2.793$ and $\gamma_n = -1.913$ are the spin gyromagnetic ratios, ξ_s and ξ_l are the renormalization constants introduced to simulate quenching of the $M1$ strength that is usually necessary for the description of the experimental data. The nonzero ξ_s and ξ_l correspond

to the effective operator $\boldsymbol{Q}$. Their standard values are (see Refs. [4,54])

$$\xi_s = 0.1, \quad \xi_l = -0.03. \tag{16}$$

Zero values

$$\xi_s = 0, \quad \xi_l = 0 \tag{17}$$

correspond to the bare operator $\boldsymbol{Q}^{(0)}$.

Equation (15) can be represented as the result of the action of the effective charge operator e_q introduced in the TFFS [2] on the bare operator $\boldsymbol{Q}^{(0)}$, that is

$$\boldsymbol{Q} = e_q \boldsymbol{Q}^{(0)}, \tag{18}$$

where

$$e_q = 1 - \tfrac{1}{2}\,(\,\xi_l\,\sigma_0\,\sigma_0' + \xi_s\,\boldsymbol{\sigma}\cdot\boldsymbol{\sigma}'\,)\,\boldsymbol{\tau}\cdot\boldsymbol{\tau}', \tag{19}$$

and σ_0 is the identity spin matrix. According to the TFFS, the operator e_q is universal, i.e., it should act on all the external field operators Q including the operators of the electric type $Q^{\rm e}$, which are proportional to σ_0. From this it follows that if we impose the condition of the invariance

$$e_q Q^{\rm e} = Q^{\rm e}, \tag{20}$$

we should set $\xi_l = 0$. The actual values of this constant used in the calculations of the magnetic excitations are very small and thus violate the condition (20) only slightly.

D. Numerical details

The equations of the RPA for the $M1$ excitations in ^{208}Pb were solved within the fully self-consistent scheme as described in Refs. [51–53]. The single-particle basis was discretized by imposing the box boundary condition with the box radius equal to 18 fm. The particle energies ε_p were limited by the maximum value $\varepsilon_p^{\max} = 100$ MeV. These conditions ensure fulfillment of the RPA energy-weighted sum rule for the isoscalar EL excitations in ^{208}Pb within 0.1 % for $L \leqslant 8$.

III. $M1$ EXCITATIONS IN ^{208}Pb IN RPA

A. Defining the problem and observables

In order to illustrate the observables for the following survey, we start with showing in Fig. 1 the distribution of $M1$ strength in ^{208}Pb calculated within self-consistent RPA based on the Skyrme EDF with two different parametrizations and comparing it with experimental data. We employ here the discrete version of the RPA because the single-particle continuum plays a minor role in the considered case. The strength functions were obtained by folding the discrete RPA spectrum and the discrete experimental mode (lower $M1$ mode) with a Lorentzian of half-width $\Delta = 20$ keV. The experimental data demonstrate the basic features of $M1$ strength in ^{208}Pb: there is a very narrow peak at lower energy $E_1 = 5.84$ MeV and a broad resonance at $E_2 = 7.39$ MeV. The height of the lower peak is characterized by its integrated $B_1(M1)$ strength equal to 2.0 μ_N^2. Experimental mean energy E_2 and summed strength $\sum B(M1)$ of the upper $M1$ resonance are computed from moments $m_k = \Sigma_\nu\, B_\nu(M1)\, E_\nu^k$ summed/integrated in the interval 6.6–8.1 MeV with the probabilities $B_\nu(M1)$ and

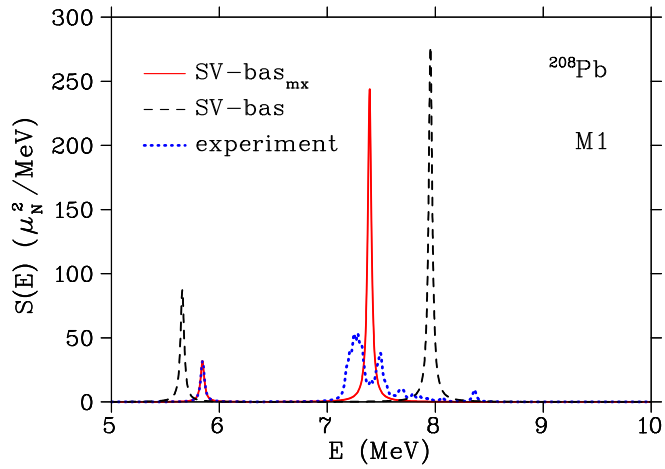

FIG. 1. Strength functions of the $M1$ excitations in ^{208}Pb calculated within RPA using the parametrization SV-bas [10] (black dashed line) and SV-bas$_{\rm mx}$ as a modified variant thereof (red solid line) introduced in Sec. IV. Experimental data taken from Refs. [13,15] are shown by the blue dotted line. The low-lying $M1$ state is at 5.84 MeV, hidden below the result from SV-bas$_{\rm mx}$. The discrete peaks from RPA and the lower $M1$ mode have been broadened with a smearing parameter $\Delta = 20$ keV to represent a smooth distribution.

the excitation energies E_ν taken from Refs. [13,15]. Note that we do not include in this interval the state with $E = 7.335$ MeV [and possible $B(M1) = 1.8\ \mu_N^2$] from Ref. [15] because of the uncertainty with the identification of its spin. We also note that the chosen smearing parameter $\Delta = 20$ keV is sufficiently large to average out the fine structure of the experimental spectrum, which is not essential for our analysis, but remains sufficiently small to resolve the spreading widths. The experimental strength distribution is composed from two data sets, below the neutron separation energy 7.37 MeV from Ref. [15] and above from Ref. [13]. It is thus not clear whether the dip between the peaks at 7.26 MeV and 7.47 MeV is a real effect. Inelastic proton scattering data [55,56] seems to indicate that the dip does not exist. Anyway, such detailed fragmentation structure cannot be described within RPA. Thus we use for comparison with RPA the average peak properties as explained above. Altogether, we have four observables $E_1 = 5.84$ MeV, $E_2 = 7.39$ MeV, $B_1(M1) = 2.0\ \mu_N^2$, and $B_2(M1) = \sum B(M1) = 15.3\ \mu_N^2$, which we use henceforth to characterize the $M1$ modes in ^{208}Pb.

Figure 1 shows theoretical results from two different parametrizations. The parametrization SV-bas$_{\rm mx}$ (which is tuned to data such that theoretical and experimental curve for the lower peak at 5.84 MeV coincide) stands at the end of our investigations and will be discussed later. The results for SV-bas (computed here with the all spin-spin terms included, i.e., $\eta_{\Delta s} = 1$) are typical for most of the available Skyrme parametrizations. They agree qualitatively in that theory also produces two dominant peaks in the correct energy range. But the position of the peaks and their strengths differs too much from the data. Reasons for that and possible cures will be discussed in the following.

B. State of the art

It is well known that the properties of the low-energy $M1$ excitations in ^{208}Pb in the RPA are mainly determined by two ph configurations formed by the neutron's (ν) and proton's (π) spin-orbit doublets $1i_{11/2}$-$1i_{13/2}$ and $1h_{9/2}$-$1h_{11/2}$. The main characteristics of these configurations are the ph energy differences. Since the single-particle spectra produced by the various parametrizations of the Skyrme EDF are very different one can trace correlations between the values of these energy differences, parameters of the EDF, and the RPA results for the $M1$ excitations in ^{208}Pb.

Let us introduce the notations:

$$\varepsilon^{\nu}_{ph} = \varepsilon^{\nu}_{p}(1i_{11/2}) - \varepsilon^{\nu}_{h}(1i_{13/2}), \tag{21}$$

$$\varepsilon^{\pi}_{ph} = \varepsilon^{\pi}_{p}(1h_{9/2}) - \varepsilon^{\pi}_{h}(1h_{11/2}), \tag{22}$$

$$\bar{\varepsilon}_{ph} = \tfrac{1}{2}\left(\varepsilon^{\nu}_{ph} + \varepsilon^{\pi}_{ph}\right), \quad \Delta\varepsilon_{ph} = \varepsilon^{\nu}_{ph} - \varepsilon^{\pi}_{ph}. \tag{23}$$

The experimental values of these quantities are: $\varepsilon^{\nu}_{ph} = 5.84$ MeV, $\varepsilon^{\pi}_{ph} = 5.55$ MeV, $\bar{\varepsilon}_{ph} = 5.70$ MeV, and $\Delta\varepsilon_{ph} = 0.29$ MeV. The theoretical values of ε^{ν}_{ph} and ε^{π}_{ph} along with the energies and the reduced probabilities of the excitation of the (isoscalar) 1^+_1 state and the mean energies and the summed strengths of the (isovector) $M1$ resonance in ^{208}Pb calculated within the self-consistent RPA for the parametrizations of the Skyrme EDF indicated in Sec. II B are presented in Fig. 2. The effective $M1$ operator (15) with the renormalization constants ξ_s and ξ_l from Eq. (16) is used. The shifts from mere ε_{ph} to the corresponding RPA energies E_n indicate the strength of residual interaction in the $M1$ channel. It is generally smaller than for the giant resonances, although still sufficiently large to be decisive. We mention in passing that the contribution of the spin-orbit term to the residual interaction is very small. The figure reveals three main problems: First, some Skyrme-EDF parametrizations used with all spin terms [that means $\eta_{\Delta s} = 1$ in Eqs. (B1) and is denoted by open circles and the label "with $s\Delta s$" in Fig. 2] lead to spin instability (imaginary RPA solutions) and thus have no entry in the plot (missing open circles). Second, the reduced probability $B_1(M1)$ of excitation of the first 1^+ state significantly exceeds its experimental value 2.0 μ_N^2 for the most parametrizations, despite the quenching produced by the effective $M1$ operator. Third, the mismatch starts already at the level of pure 1ph energies ε^{ν}_{ph}, which are definitely too large [Fig. 2(b)], which can be tracked down to the fact that all parametrizations give too large values of $\Delta\varepsilon_{ph}$ as compared to the experiment (see Fig. 3). As a result, none of the parametrizations listed in Fig. 2 gives a satisfactory description of both $M1$ modes simultaneously. These problems were already found in earlier publications and the spin-orbit coupling was identified as one mechanism driving the $M1$ properties [21,22]. We will now discuss that in more detail and explore ways for a solution.

C. Spin stability

Spin stability is a crucial issue in the construction of Skyrme parametrizations [44,57]. The first is to check the stability of bulk matter, which is done easily in terms of the LM parameters of the residual interaction. The LM parameters

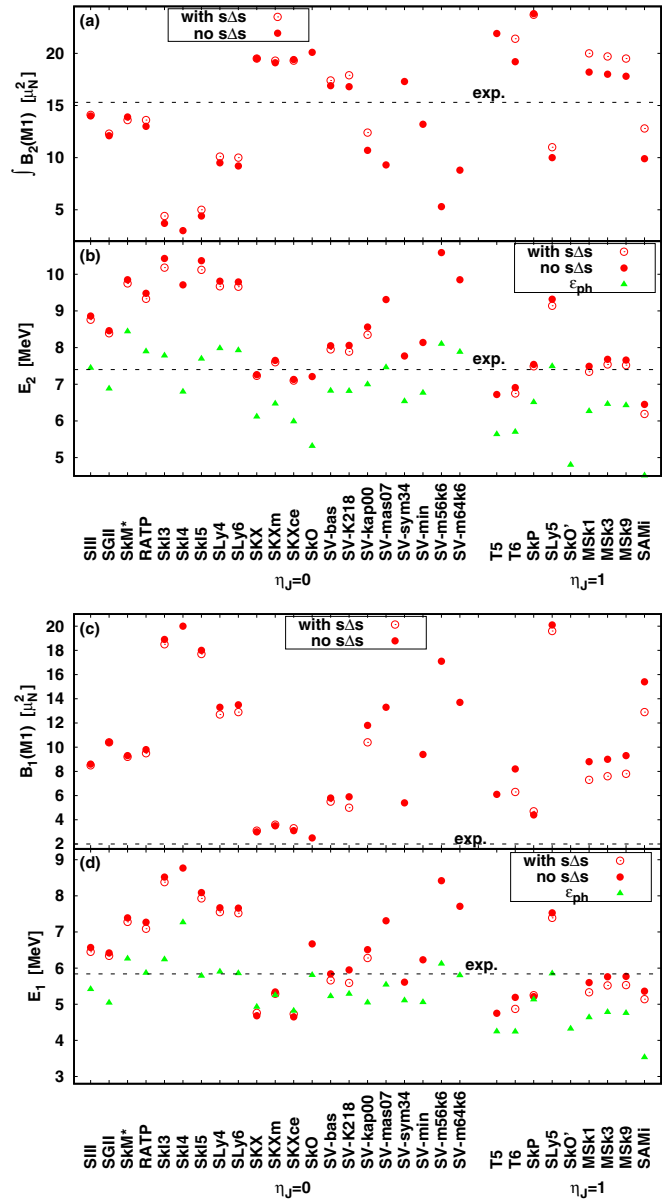

FIG. 2. RPA results for the $B_n(M1)$ values [(a) and (c)] and the energies E_n [(b) and (d)] of the two leading $M1$ modes in ^{208}Pb for a variety of published Skyrme-EDF parametrizations as listed in Sec. II B. For the energies, we show also the leading 1ph excitations ε^{ν}_{ph} [(b)] and ε^{π}_{ph} [(d)]. Experimental values of $B_n(M1)$ and E_n are indicated by horizontal dotted lines. The parametrizations are grouped in those that omit tensor spin-orbit ($\eta_J = 0, C^J_T = 0$) and those that use it ($\eta_J = 1, C^J_T \neq 0$). RPA results are considered for two options concerning the spin gradient terms $\propto s\Delta s$: $\eta_{\Delta s} = 1$ ($C^{\Delta s}_T \neq 0$) and $\eta_{\Delta s} = 0$ ($C^{\Delta s}_T = 0$).

are related with the C constants of the Skyrme-EDF by the following equations (see, e.g., Refs. [58,59])

$$F_0 = 2N_0\left[C^{\rho}_0 + \tfrac{1}{2}(\alpha+1)(\alpha+2)C^{\rho,\alpha}_0\rho^{\alpha}_{\rm eq} + C^{\tau}_0 k^2_{\rm F}\right], \tag{24a}$$

$$F'_0 = 2N_0\left[C^{\rho}_1 + C^{\rho,\alpha}_1\rho^{\alpha}_{\rm eq} + C^{\tau}_1 k^2_{\rm F}\right], \tag{24b}$$

$$G_0 = 2N_0\left[C^{s}_0 + C^{s,\alpha}_0\rho^{\alpha}_{\rm eq} - C^{J}_0 k^2_{\rm F}\right], \tag{24c}$$

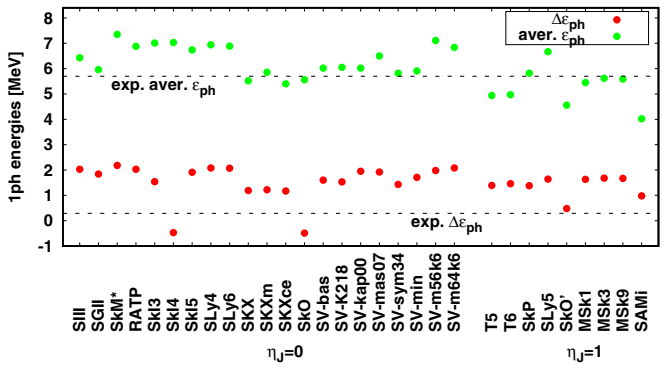

FIG. 3. Average 1ph energy and difference as defined in Eq. (23) for the same selection of published Skyrme parametrizations as in Fig. 2. Experimental values are indicated by horizontal dotted lines.

$$G_0' = 2N_0\left[C_1^s + C_1^{s,\alpha}\rho_{\rm eq}^{\alpha} - C_1^J k_{\rm F}^2\right], \tag{24d}$$

$$F_1 = -2N_0 C_0^\tau k_{\rm F}^2, \quad F_1' = -2N_0 C_1^\tau k_{\rm F}^2, \tag{24e}$$

$$G_1 = 2N_0 C_0^J k_{\rm F}^2, \quad G_1' = 2N_0 C_1^J k_{\rm F}^2, \tag{24f}$$

where $N_0 = 2m^* k_{\rm F}/(\pi\hbar)^2$, $k_{\rm F} = (3\pi^2\rho_{\rm eq}/2)^{1/3}$ is the Fermi momentum, and $\rho_{\rm eq}$ is the equilibrium density of the infinite nuclear matter (INM). Equations (24) coincide with the definitions of Ref. [39] if the C constants are expressed through the parameters of the Skyrme force by the standard formulas. However, Eqs. (24) produce G_L and G_L' at variance with Ref. [39] for those parametrizations in which the J^2 terms are omitted ($\eta_J = 0$ and $C_T^J = 0$) as noted in Ref. [60]. In particular, the parameters G_1 and G_1' are exactly equal to zero if the J^2 terms are absent in the Skyrme EDF. To ensure stability, the LM parameters should satisfy the following inequalities (see Ref. [2])

$$\frac{F_L}{2L+1} > -1, \quad \frac{F_L'}{2L+1} > -1, \tag{25a}$$

$$\frac{G_L}{2L+1} > -1, \quad \frac{G_L'}{2L+1} > -1. \tag{25b}$$

Table I shows the LM parameters corresponding to the Skyrme-EDF parametrizations listed in Fig. 2. The values of the spin-orbit parameter x_W, which will be discussed in Sec. III D are also given. The conditions (25) are fulfilled for all parameters from Table I except for the parameter G_0 of SkO′. However, as can be seen from Fig. 2, the parametrizations T5, SkI4, SkO, SV-mas07, SV-sym34, SV-min, SV-m56k6, and SV-m64k6, for which the INM is stable, lead to

TABLE I. Landau-Migdal parameters of the Skyrme-EDFs listed in Fig. 2.

EDF	η_J	x_W	F_0	F_0'	G_0	G_0'	F_1	F_1'	G_1	G_1'	N_0^{-1} (MeV fm^3)	m^*/m	$k_{\rm F}$ (fm^{-1})
SIII	0	1	0.31	0.87	0.54	0.95	−0.71	0.49	0	0	207.8	0.76	1.29
SGII	0	1	−0.23	0.73	0.62	0.93	−0.64	0.52	0	0	196.1	0.79	1.33
SkM*	0	1	−0.23	0.93	0.33	0.94	−0.63	0.62	0	0	194.6	0.79	1.33
RATP	0	1	−0.28	0.59	0.63	0.89	−1.00	0.56	0	0	230.2	0.67	1.33
T5	1	1	−0.10	1.96	−0.88	0.05	−0.00	−0.00	0.97	0.97	152.3	1.00	1.34
T6	1	1	0.06	1.43	−0.22	0.18	−0.00	−0.00	0.86	0.86	153.3	1.00	1.34
SkP	1	1	−0.10	1.42	−0.23	0.06	0.00	1.05	−0.18	0.97	152.7	1.00	1.34
SkI3	0	0	−0.32	0.65	1.90	0.85	−1.27	−0.84	0	0	267.2	0.58	1.33
SkI4	0	−0.99	−0.27	0.56	1.77	0.88	−1.05	−0.57	0	0	236.4	0.65	1.33
SkI5	0	1	−0.32	0.76	1.79	0.85	−1.26	−0.84	0	0	267.7	0.58	1.32
SLy4	0	1	−0.28	0.81	1.39	0.90	−0.92	−0.40	0	0	221.2	0.69	1.33
SLy5	1	1	−0.28	0.81	1.12	−0.14	−0.91	−0.39	0.25	1.04	220.1	0.70	1.33
SLy6	0	1	−0.28	0.80	1.41	0.90	−0.93	−0.41	0	0	223.0	0.69	1.33
SKX	0	0	0.24	1.56	−0.46	1.04	−0.02	0.98	0	0	156.1	0.99	1.32
SKXm	0	0	0.05	1.47	−0.29	1.02	−0.10	0.87	0	0	159.4	0.97	1.33
SKXce	0	0	0.24	1.52	−0.45	1.04	0.02	1.01	0	0	154.1	1.01	1.32
SkO	0	−1.13	−0.10	1.33	0.48	0.98	−0.31	0.16	0	0	171.2	0.90	1.33
SkO′	1	−0.58	−0.10	1.33	−1.61	0.79	−0.31	0.09	2.16	0.19	171.3	0.90	1.33
MSk1	1	1	0.07	1.47	−0.18	0.25	−0.00	−0.00	0.78	0.78	154.3	1.00	1.33
MSk3	1	1	0.07	1.30	−0.00	0.27	−0.00	−0.00	0.77	0.77	154.3	1.00	1.33
MSk9	1	1	0.07	1.30	−0.02	0.25	−0.00	−0.00	0.78	0.78	154.3	1.00	1.33
SV-bas	0	0.55	−0.05	1.20	0.00	0.99	−0.30	0.78	0	0	170.8	0.90	1.33
SV-K218	0	0.45	−0.12	1.18	0.02	0.99	−0.30	0.77	0	0	170.3	0.90	1.34
SV-kap00	0	1.33	−0.05	1.20	1.08	0.99	−0.30	−0.30	0	0	170.8	0.90	1.33
SV-mas07	0	1.02	−0.26	0.71	1.16	0.90	−0.90	−0.06	0	0	219.5	0.70	1.33
SV-sym34	0	0.29	−0.04	1.50	−0.29	0.99	−0.30	0.78	0	0	170.9	0.90	1.33
SV-min	0	0.83	−0.05	1.37	0.58	1.01	−0.14	0.07	0	0	160.9	0.95	1.34
SV-m56k6	0	0.79	−0.35	0.24	1.78	0.84	−1.33	−0.33	0	0	277.4	0.56	1.33
SV-m64k6	0	1.10	−0.30	0.40	1.30	0.87	−1.09	0.05	0	0	242.3	0.64	1.33
SAMi	1	0.31	−0.25	0.56	0.15	0.35	−0.97	0.05	1.03	0.54	228.0	0.68	1.33

the spin instability of the ground state of ^{208}Pb in the case of $\eta_{\Delta s} = 1$, in spite of bulk stability as proven by Table I. This instability appears only in certain finite nuclei and is generated by the spin surface terms $\propto C_T^{\Delta s}$, not contained in Eqs. (24) for the LM parameters (see also Ref. [61] where this question is discussed in more detail). On the other hand, Fig. 2 shows that the inclusion of the terms proportional to $C_T^{\Delta s}$ into the Skyrme EDF usually decreases the energy of the 1_1^+ state (compare open with filled circles). Exceptions from this general trend are SkP, SKX, and SKXce for which $E(1_1^+)$ slightly increases if $\eta_{\Delta s} = 1$. If the downshift by the $C_T^{\Delta s}$ terms grows too large, it drives the finite nucleus to instability. All the Skyrme-EDF parametrizations shown in Fig. 2 except for SkO′ provide a stable ground state for ^{208}Pb in case of $\eta_{\Delta s} = 0$, which is in agreement with the INM properties resulting from Table I.

Note that the instability generated by the EDF SkO′ disappears in the modified parametrization SkO′$_{\rm m}$, in which the C constants are determined by Eqs. (B1) with $\eta_s = \eta_{s,\alpha} = \eta_{\Delta s} = 0$, $C_{\rm N} = 300$ MeV $\cdot$ fm^3, $g = 0.891$, and $g' = 1.39$. In this case we have $G_0 = -0.60$, $G_0' = 2.24$. The parameters $F_{0,1}$, $F_{0,1}'$, G_1, and G_1' are not changed. Thus, the nuclear matter becomes stable. The parameters g and g' in SkO′$_{\rm m}$ have been adjusted to reproduce within the RPA the experimental energies of the $M1$ excitations in ^{208}Pb, $E_1 = 5.84$ MeV and $E_2 = 7.39$ MeV. The $B(M1)$ values for the 1_1^+ state and the isovector $M1$ resonance in ^{208}Pb in this parametrization are equal to 1.9 μ_N^2 and 16.9 μ_N^2, respectively.

D. Impact of spin-orbit parameters

Figure 2 indicates that problems appear already at the level of the 1ph energies. This becomes even more apparent when looking at the average and difference 1ph energies (23) as shown in Fig. 3. First, the most parametrizations have the spin-orbit parameter $x_W \geqslant 0$, and for them the calculated value of $\Delta\varepsilon_{ph}$ exceeds the experimental value (0.29 MeV) by a factor of 3.4 (SAMi) to 7.5 (SkM*). In the case of parametrizations with $x_W < 0$ (they are SkI4, SkO, and SkO′, see Table I), the value of $\Delta\varepsilon_{ph}$ considerably decreases, becoming negative for SkI4 and SkO. This demonstrates the well-known fact that the value of x_W is one of the key agents for the spin-orbit splitting (see Refs. [21,22] where this question was considered in terms of the parameter $b_4' = x_W W_0/2$). Second, for the parametrizations with $x_W > 0$, the value of $B_1(M1)$ calculated with $\eta_{\Delta s} = 0$ is greater than its experimental value (2.0 μ_N^2) by a factor of 2.2 (SkP) to 10 (SLy5). This together suggests that the values of x_W and $\Delta\varepsilon_{ph}$ should also have a strong influence on the RPA results for the $M1$ excitations in ^{208}Pb.

To explore this further, we consider simultaneous variation of the spin-orbit parameters x_W and W_0. In other words, we keep the ph interaction approximately fixed and vary the 1ph energies. (This is possible because the $M1$ results in ^{208}Pb depend practically only on the two spin-orbit doublets and because the residual interaction V only slightly depends on the spin-orbit parameters). To that end, we start from the set SV-bas [10], vary x_W, keeping all other model parameters frozen, and tune W_0 to reproduce the SHF binding energy of ^{208}Pb at its experimental value 1636.43 MeV within the accuracy of 0.2 MeV. This is done for the option $\eta_{\Delta s} = 1$.

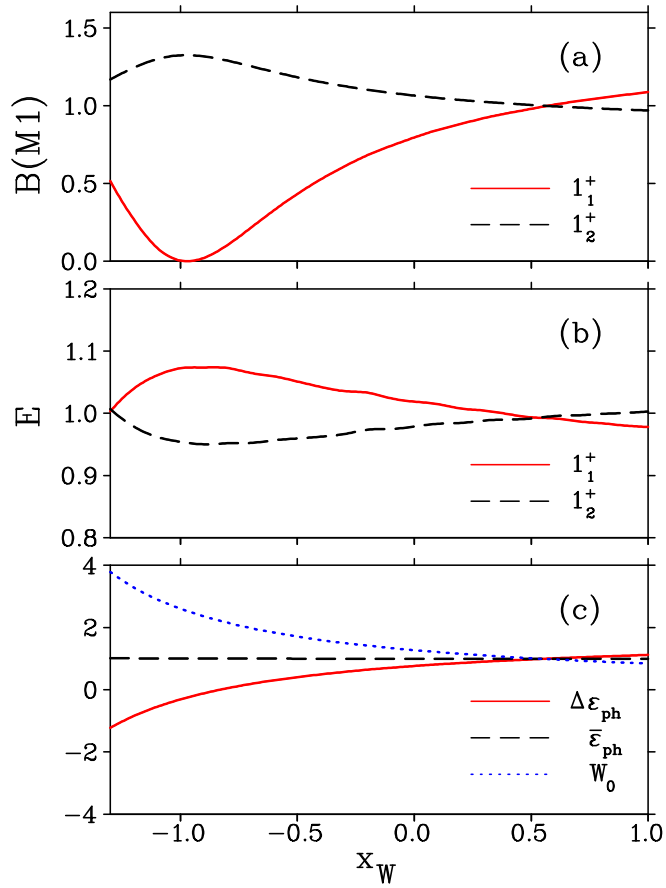

FIG. 4. Dependence of the characteristics of $M1$ excitations in ^{208}Pb on the parameter x_W of the Skyrme EDF. Parametrization SV-bas [10] is used. (a) The reduced probabilities $B(M1)$ of the excitation of the first (solid red line) and second (dashed black line) 1^+ states calculated in the RPA. (b) Same as in (a) but for the energies of these states. (c) The values of the energy differences $\Delta\varepsilon_{ph}$ (solid red line) and $\bar{\varepsilon}_{ph}$ (dashed black line), Eqs. (23), and the spin-orbit parameter W_0 (dotted blue line). All the quantities are given in units of their values obtained for the original parametrization [10]. See text for more details.

Figure 4 shows the dependence of the RPA results for the first and second 1^+ states in ^{208}Pb on the parameter x_W obtained in this way. The respective values of $\Delta\varepsilon_{ph}$, $\bar{\varepsilon}_{ph}$, and W_0 are also shown. All these quantities are given in units of their values obtained for the original set SV-bas [10] and shown in Figs. 2 and 3 [$B_1(M1) = 5.5$ μ_N^2, $B_2(M1) = 17.4$ μ_N^2, $E_1 = 5.66$ MeV, $E_2 = 7.95$ MeV, $\Delta\varepsilon_{ph} = 1.60$ MeV, $\bar{\varepsilon}_{ph} = 6.02$ MeV] and the value $W_0 = 124.634$ MeV $\cdot$ fm^5. The $B_1(M1)$ shows the strongest dependence on x_W. This is due to the fact that in the case of the $M1$ operator (15), the proton's and the neutron's contributions to the amplitudes $\langle Z^n \,|\, Q^{\alpha}_{L_n M_n}\rangle$ in Eq. (7) for the reduced probabilities have the opposite signs for $B_1(M1)$ and the equal signs for $B_2(M1)$. Actually, one can obtain any value of $B_1(M1) < 6$ μ_N^2 by decreasing the parameter x_W. The experimental value $B_1(M1) = 2.0$ μ_N^2 is obtained at $x_W < 0$. The values of E_1, E_2, and $B_2(M1)$ depend on x_W to much lesser extent. The energy difference $\Delta\varepsilon_{ph}$ also shows a strong dependence on x_W, while the value of $\bar{\varepsilon}_{ph}$ is

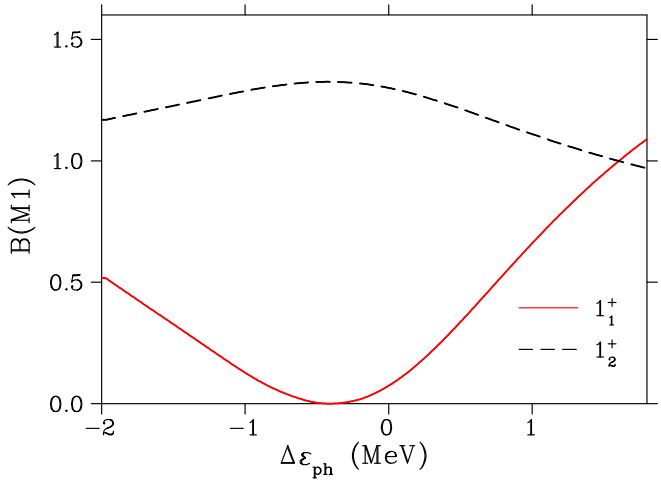

FIG. 5. Same as in Fig. 4 but for the dependence of the reduced probabilities $B(M1)$ on the value of the energy difference $\Delta\varepsilon_{ph}$.

nearly constant (it is changed within 2.2% in the considered interval of x_W). The trend of $\Delta\varepsilon_{ph}$ with x_W is monotonous. This allows to transform the dependencies shown in Figs. 4(a) and 4(b) into analogous dependencies on $\Delta\varepsilon_{ph}$. The results are shown in Fig. 5, where again we see the crucial dependence of $B_1(M1)$ on $\Delta\varepsilon_{ph}$ at the constant $\bar{\varepsilon}_{ph}$. This dependence explains why the parametrization $\mathrm{SkO}'_{\mathrm{m}}$ introduced in Sec. III C gives nice agreement with the experimental value of $B_1(M1)$: it has negative $x_W = -0.58$ and thus a value of $\Delta\varepsilon_{ph} = 0.48$ MeV, which is closest to the experimental value 0.29 MeV. The other Skyrme-EDF parametrizations have generally too large $\Delta\varepsilon_{ph}$ which leads to significant overestimation of the $B_1(M1)$.

The impact of the value of $\Delta\varepsilon_{ph}$ on the properties of $M1$ excitations in ^{208}Pb was already pointed out in Refs. [21,22]. This value characterizes the isotopic properties of the spin-orbit interaction. Notice that the questions concerning the form and the parameters of the spin-orbit terms of the Skyrme force were discussed since the original papers on this topic (see Refs. [34,35]). In Refs. [43,62,63] it was shown that there is a significant difference between the isospin dependence of the spin-orbit terms in the relativistic mean-field (RMF) and the nonrelativistic Skyrme models and that the RMF results correspond to the value $x_W \simeq 0.1$ of the Skyrme-EDF parameter. Another possible options for more flexibility in the spin-orbit terms of the one-body potential were discussed in Refs. [64,65], however, at the price of breaking isospin symmetry.

IV. TOWARD BETTER REPRODUCTION OF $M1$ MODES

The results presented in Sec. III D show that spin-orbit parameters are most decisive for the $M1$ modes mediated through the 1ph spin-orbit splittings while their influence in the residual interaction is negligible. And, of course, the parameters of the spin-spin terms play an equally important role, here, however, exclusively through the residual interaction. This motivates us to check the chances to find a Skyrme functional in standard form, which provides a good description of $M1$ modes together with traditionally good modeling of ground-state properties. At present stage, it is too early to launch a fully fledged least-squares fitting scheme [10,66,67] particularly because a high-precision RPA computation of $M1$ modes is far too expensive. Thus, for a first exploration, we employ a simple, restricted fitting procedure: We start from a given Skyrme parametrization, keep all model parameters at their given value except for the spin-orbit parameters $C_T^{\nabla J}$ (alias x_W, W_0) and the spin-spin parameters C_T^s, $C_T^{s,\alpha}$, and $C_T^{\Delta s}$. The spin-spin parameters play no role for ground states of even-even nuclei. Thus we exploit here the freedom of not yet fixed parameters. However, the spin-orbit parameters enter ground-state properties. Here we have to check that retuning does not destroy ground-state quality.

TABLE II. Parameters η_J, x_W, W_0, g, and g' of the modified Skyrme EDFs. Parameters g and g' of the Landau-Migdal interaction (13) are taken from Ref. [19]. All Landau-Migdal parameters are normalized to $C_{\mathrm{N}} = 300$ MeV $\cdot$ fm^3.

EDF	η_J	x_W	W_0 (MeV fm^5)	g	g'
$\mathrm{SkM}^*_{\mathrm{m}}$	0	−0.65	295	−0.366	−0.015
$\mathrm{SLy4}_{\mathrm{m}}$	0	−0.62	275	−0.308	0.102
$\mathrm{SV\text{-}bas}_{\mathrm{mx}}$	0	−0.50	213	−0.028	0.516
$\mathrm{SV\text{-}bas}_{\mathrm{m}}$	0	−0.55	221	−0.037	0.518
$\mathrm{SV\text{-}K218}_{\mathrm{m}}$	0	−0.54	220	−0.040	0.520
$\mathrm{SV\text{-}kap00}_{\mathrm{m}}$	0	−0.57	225	−0.040	0.520
$\mathrm{SV\text{-}mas07}_{\mathrm{m}}$	0	−0.59	244	−0.159	0.335
$\mathrm{SV\text{-}sym34}_{\mathrm{m}}$	0	−0.68	244	0.027	0.645
$\mathrm{SV\text{-}min}_{\mathrm{m}}$	0	−0.57	222	−0.003	0.590
$\mathrm{SV\text{-}m56k6}_{\mathrm{m}}$	0	−0.56	258	−0.303	0.118
$\mathrm{SV\text{-}m64k6}_{\mathrm{m}}$	0	−0.52	239	−0.235	0.205
$\mathrm{SkP}_{\mathrm{m}}$	1	−0.26	175	−0.013	0.630
$\mathrm{SLy5}_{\mathrm{m}}$	1	−0.19	212	−0.151	0.463
Landau-Migdal				0.1	0.75

To keep the number of free spin-spin parameters low, we set $\eta_{s,\alpha} = \eta_{\Delta s} = 0$ and determine C_T^s by Eqs. (B1) with $\eta_s = 0$ and the fitting parameters g and g' at $C_{\mathrm{N}} = 300$ MeV $\cdot$ fm^3. After all, we have four free parameters x_W, W_0, g, and g', which are determined by adjusting four observables in ^{208}Pb: the binding energy and the RPA results for the $M1$ energies E_1 and E_2 and the transition probability $B_1(M1)$ to their experimental values (see Sec. III A). Note that here we use, as before, the effective $M1$ operator (15) with the renormalization constants ξ_s and ξ_l from Eq. (16). This fitting procedure is applied to a subset of the parametrizations shown in Figure 2. The modified parametrizations thus obtained are marked by an index "m". Resulting retuned model parameters and properties of $M1$ modes are shown in Fig. 6 and the corresponding retuned spin-orbit and spin-spin parameters are given in quantitative detail in Table II. As expected from the exploration in Sec. III D, all retuned x_W parameters are negative, most of them in the interval between −0.6 and −0.5. Exceptions are $\mathrm{SkP}_{\mathrm{m}}$ and $\mathrm{SLy5}_{\mathrm{m}}$ which have higher x_W due to the J^2 terms in these parametrizations, which contribute also to the single-particle spin-orbit potential. The retuned parameters W_0 are all rather large. This seemingly happens

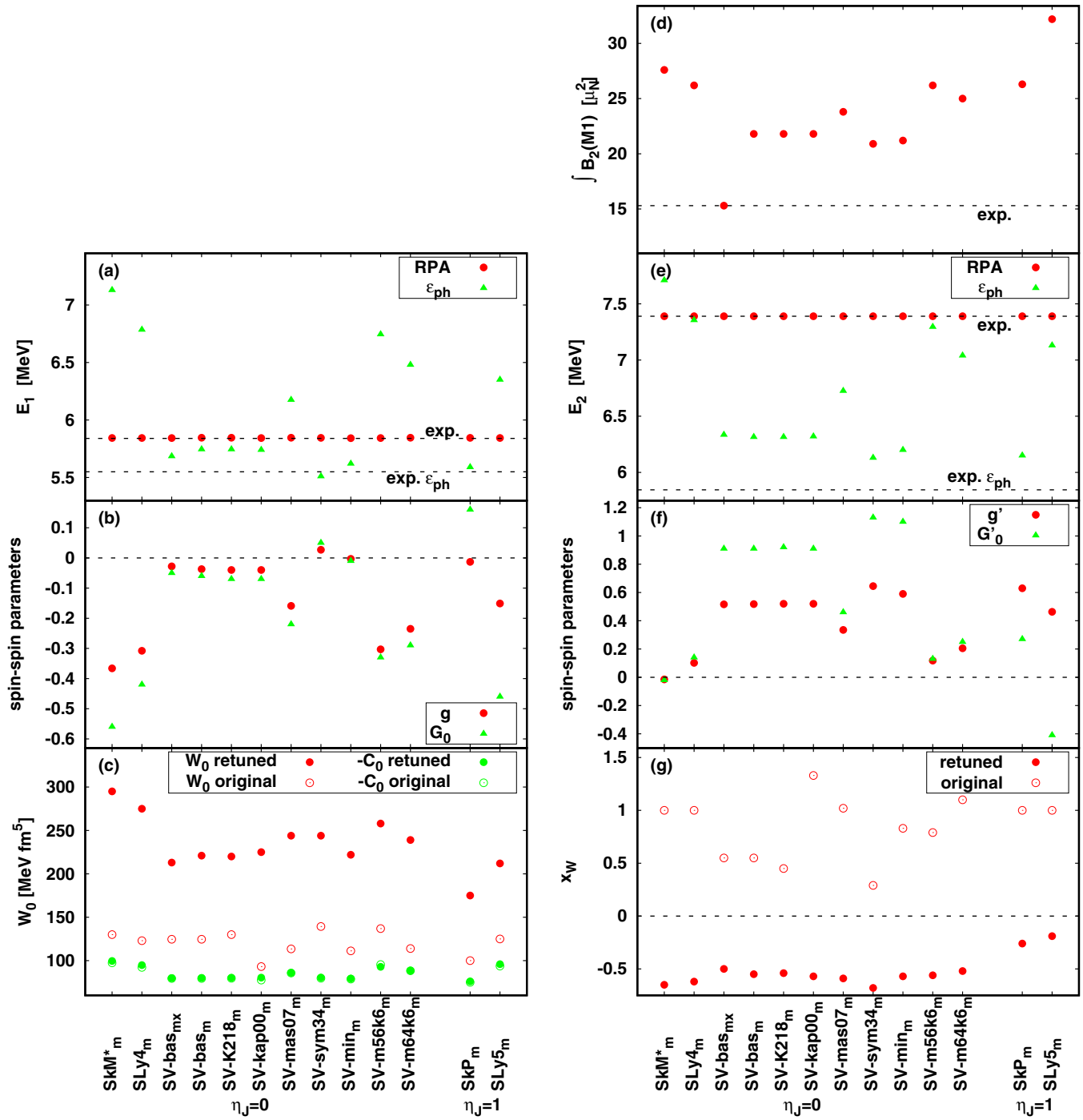

FIG. 6. Results for the retuned parametrizations. (a) and (e) The $M1$ energies E_1 and E_2 together with their corresponding 1ph energies ε^{π}_{ph} and ε^{ν}_{ph}. (d) The $B(M1)$ strength for the upper $M1$ mode integrated over the interval 6.6–8.1 MeV. Experimental values are indicated by horizontal faint dashed lines. (b) and (f) Spin-spin LM parameters G_0 and G'_0 together with the interaction parameters g and g' defined in Eqs. (B1). (c) and (g) Retuned values (filled circles) of the spin-orbit parameters W_0, x_W, and $-C_0^{\nabla J}$ (abbreviated $-C_0$ in the legend) together with their original values (open circles).

to compensate the negative x_W. Figure 6(c) shows also the isoscalar spin-orbit parameter $C_0^{\nabla J} = -\frac{1}{4}(2 + x_W)W_0$. This combination shows much less variations over the different forces and, in particular, remains practically unmodified by retuning. It is the isovector spin-orbit term proportional to $C_1^{\nabla J} = -\frac{1}{4}x_W W_0$, which makes the difference. Seeing the dramatic differences in spin-orbit parameters, one wonders what happens to the overall quality of the parametrization. This question will be addressed further below.

The spin-spin coupling parameters g and g' show some correlation with the effective mass m^*/m of a parametrization. The sets SkP$_m$, SV-bas$_m$, SV-K218$_m$, SV-kap00$_m$,

SV-sym34$_{\rm m}$, and SV-min$_{\rm m}$ all having $m^*/m \approx 1$ have similar values, which are also close to the values $g = 0.1$, $g' = 0.75$ used previously in the non-self-consistent TFFS (see Ref. [19]) while the other parametrizations having lower m^*/m also produce lower g and g'.

The LM parameters G_0 and G'_0 in Figs. 6(b) and 6(f) stay all safely above -1 and thus lead to stable INM, which also persists in finite nuclei because the modified parametrizations set the critical gradient spin term to zero.

The RPA energies E_n stay by construction at the experimental values. We show them in Figs. 6(a) and 6(e) to illustrate the span toward the pure 1ph energies ε^{π}_{ph} [Fig. 6(a)] and ε^{ν}_{ph} [Fig. 6(e)]. Let us concentrate first on the isoscalar mode, Fig. 6(a). The upshift by the residual interaction is small for the parametrizations with $m^*/m \approx 1$, in accordance with the small values of g or G_0. In these cases, the 1ph energies represent already a good estimate of E_1 and the theoretical ε^{π}_{ph} lie close to the experimental value (faint dotted line). Lower effective masses increase ε^{π}_{ph}, away from the wanted E_1, and need more residual interaction to compensate. The impact of residual interaction is much larger for the isovector modes, Fig. 6(e), again in accordance with the much larger spin coupling parameter g'. In that case, we also have the problem that all theoretical ε^{ν}_{ph} are much higher than the experimental value of 5.84 MeV.

Figure 6(d) shows the $B(M1)$ strength integrated over the vicinity of the upper $M1$ mode. One observes a close relation between g' and the isovector $B(M1)$ value: An increase of g' reduces the $B(M1)$ value. This is due to the increase of the ground-state correlations (Y-components of the RPA transition amplitudes), which decreases the transition probabilities in the magnetic case in contrast to the electric case where the ground-state correlations add coherently. The parametrizations SkP$_{\rm m}$ and SLy5$_{\rm m}$ behave slightly different because as mentioned before in these parametrizations the J^2 terms are included. These terms have a noticeable impact on the $B(M1)$ values that can be estimated with the help of the single-particle part of the RPA energy-weighted sum rule (EWSR) $m_1^{\rm s.p.}$. In the case of the $M1$ excitations with the operator (15) it has the form

$$m_1^{\rm s.p.} = \tfrac{1}{2}\,{\rm Tr}\,(\rho\,[[\boldsymbol{Q},\,h\,],\cdot\boldsymbol{Q}\,]) \tag{26}$$

(see Ref. [68] for more details). In our self-consistent RPA calculations we obtain that this EWSR is fulfilled within 0.2% in the case of the Skyrme-EDF parametrizations without the J^2 terms ($\eta_J = 0$). In the case of the SkP$_{\rm m}$ and SLy5$_{\rm m}$ parametrizations ($\eta_J = 1$), this EWSR is exceeded by 19% and 25%, respectively.

Generally, we see in Fig. 6(d) that the theoretical isovector $B(M1)$ strengths, even for the best parameter sets, are significantly larger than the experimental values. Here one has to bear in mind that the experimental data in Fig. 6 have been integrated only up to 8.1 MeV. We know from previous beyond-RPA calculations within the Landau-Migdal approach [31] that the theoretical strength is distributed by coupling to 2ph states up to much higher energies. Such spectral fragmentation is also seen in data. A recent (p,p') experiment [55,56] reports a summed $B(M1) = 20.5(1.3)\ \mu_N^2$ when integrated up to 9 MeV, a value that would fit nicely into the theoretical results of Fig. 6. This situation reminds us at the case of the Gamow-Teller resonance in ^{208}Pb where only half of the sum-rule strength was concentrated in one single strong resonance and the rest was missing. Calculations within a 2ph model [69] (where one of the authors was involved) predicted a long tail, which included the other half of the total strength. Ten years later the predicted strength had been detected experimentally. Thus, excess of the strength can be corrected in extended RPA models including particle-phonon coupling that give also rise to a shift of the RPA strength to higher energies.

So far, we have computed the $B(M1)$ strengths with the effective $M1$ operator using the renormalization constants ξ_s and ξ_l as defined in Eq. (16). This construction is designed to account for correlation effects not included in the actual Hilbert space. Thus the ξ_s and ξ_l can, in principle, be different for the different models. This was exploited in the variant SV-bas$_{\rm mx}$ where ξ_s was used tentatively as further free parameter and the isovector $B(M1)$ strength as additional data point. The fitted renormalization constants for SV-bas$_{\rm mx}$ are $\xi_s = 0.154$ while $\xi_l = 0$ is chosen in accordance with the condition (20). The results in Fig. 6 shows that this strategy allows to produce better $B(M1)$ strength while maintaining the quality of the other observables. Note that the changes in ξ_s and ξ_l are, in fact, small, which rather supports the original choices (16). Anyway, this fit of renormalization constants should be considered as an exploration of still loose ends in modeling. Playing with these values needs yet to be supported by sound many-body theory.

As argued above, spin-orbit parameters have not only huge impact on $M1$ modes, but also on ground-state properties. Thus a dramatic change of isovector spin-orbit coupling as implied in the retuned parametrizations could have unwanted side effects on the quality concerning the reproduction of ground-state characteristics. Figure 7 shows the performance of the refitted parametrizations with respect to ground-state energy and charge radius. The change of spin-orbit parameters leaves the overall quality basically conserved. There is no effect at all for the radii. Energy reacts more sensitively, which is a little surprise because pairing in semimagic nuclei is highly sensitive to level density, which, of course, is influenced by spin-orbit splitting. Note that particularly the more recent, well-fitted parametrizations show a loss of energy quality, fortunately in acceptable bounds. Still, the simple minded retuning strategy spoils somewhat the overall quality of the parametrizations, the better the quality originally the larger the loss. Moreover, there are more subtle observables as pairing gaps and isotopic shifts of radii. The latter are known to be sensitive to the isovector spin-orbit term [43], for pairing gaps it is likely. All this calls for more continued investigations, more systematic fits, and correlation analysis [67] to clearly work out the impact of information from $M1$ modes on nuclear density functionals.

So far, we have discussed the properties of $M1$ modes in terms of two energies and $B(M1)$ values. Let us finally look again at the whole spectral distribution as it was shown in Fig. 1. The results obtained with the freshly retuned parametrization SV-bas$_{\rm mx}$ agree, by construction, nicely with experimental data. Comparison with the original SV-bas

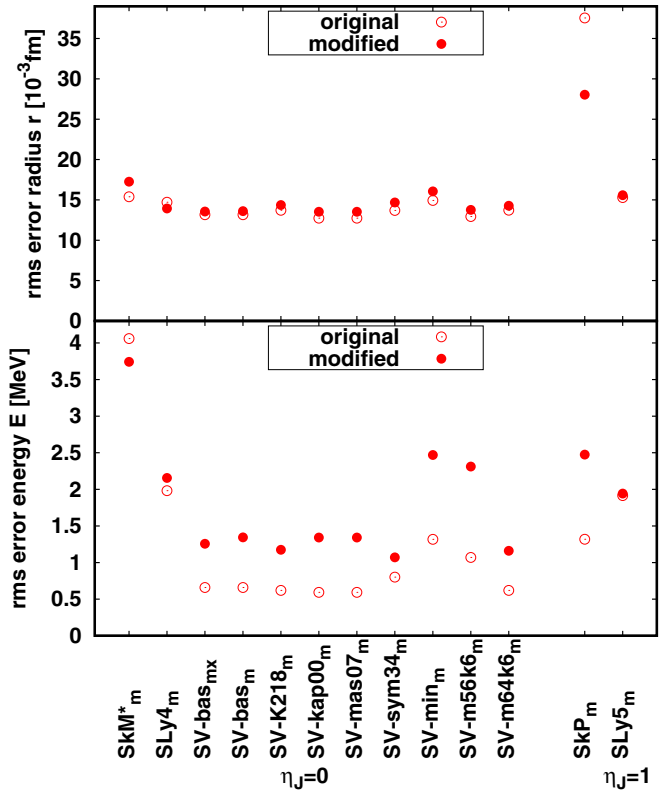

FIG. 7. Average quality of the retuned parametrizations quantified in terms of root-mean-square deviation of energy and charge radii taken over the set of spherical nuclei from Ref. [10].

shows the gain. Similar plots would be obtained when comparing original and retuned versions of the other parametrizations. But Fig. 1 also points toward the yet open problems with the upper $M1$ mode: First, the strength is overestimated, and second, its spectral fragmentation is not described at all. Both problems are related to each other as discussed above. The hope is that a beyond-RPA modeling within the phonon-coupling model could deliver the missing pieces.

V. CONCLUSIONS

In the present paper, we have investigated the impact of the spin-dependent part of the Skyrme energy density functional (EDF) on magnetic excitation modes computed within the self-consistent random-phase approximation (RPA). We considered here, in particular, magnetic dipole ($M1$) modes in ^{208}Pb as test case. The $M1$ modes are found to depend crucially on the spin-orbit term and on the spin-spin interaction. The latter has no influence on ground-state properties and generally only weak relations to natural-parity modes in even nuclei and is thus open to adjustment. The spin-orbit term is to some extent constrained by ground-state properties. However, we find that ground states leave enough leeway in them to accommodate the properties of $M1$ modes with only small sacrifices on the overall quality of the ground-state properties. We have tested that on a variety of 12 published Skyrme EDFs.

In the analysis, we were guided by the Landau-Migdal (LM) parameters from the theory of finite Fermi systems (TFFS), which are weak in the isoscalar spin part and strongly repulsive in the isovector part. The retuned Skyrme EDFs deliver LM parameters in accordance with the TFFS. The relations between the LM parameters and the parameters of the Skyrme-EDF serve also for a quick first check of spin stability of the chosen parameter set.

As open questions remain the fragmentation and the magnitude of the isovector $M1$ resonance. Both are connected with more complex configurations beyond RPA, e.g., the coupling to the low-lying phonons (strong modes in each angular momentum channel). This, however, requires that all relevant phonons, also in the magnetic channels, are correctly described by RPA. The present survey is a first step toward a proper description of magnetic excitations in the framework of Skyrme-EDF and so paves the way to subsequent beyond-RPA calculations.

ACKNOWLEDGMENTS

V.T. and N.L. acknowledge financial support from the Russian Science Foundation (Project No. 16-12-10155). Research was carried out using computational resources provided by Resource Center “Computer Center of SPbU”.

APPENDIX A: LOCAL DENSITIES AND CURRENTS

Let us introduce the isoscalar ($T=0$) and isovector ($T=1$) single-particle density matrices

$$\rho_T(\boldsymbol{r},\sigma;\boldsymbol{r}',\sigma') = \rho_n(\boldsymbol{r},\sigma;\boldsymbol{r}',\sigma') + (-1)^T \rho_p(\boldsymbol{r},\sigma;\boldsymbol{r}',\sigma'), \quad \text{(A1)}$$

where $\rho_n(\boldsymbol{r},\sigma;\boldsymbol{r}',\sigma')$ and $\rho_p(\boldsymbol{r},\sigma;\boldsymbol{r}',\sigma')$ are the neutron's and proton's density matrices. The expressions for the local densities and currents entering Eq. (12) in terms of these matrices read

$$\rho_T(\boldsymbol{r}) = \sum_\sigma \rho_T(\boldsymbol{r},\sigma;\boldsymbol{r},\sigma), \quad \text{(A2)}$$

$$\tau_T(\boldsymbol{r}) = \sum_\sigma \nabla\cdot\nabla'\,\rho_T(\boldsymbol{r},\sigma;\boldsymbol{r}',\sigma)|_{\boldsymbol{r}=\boldsymbol{r}'}, \quad \text{(A3)}$$

$$\boldsymbol{J}_T(\boldsymbol{r}) = i\sum_{\sigma,\sigma'} [(\boldsymbol{\sigma})_{\sigma',\sigma}\times\nabla]\,\rho_T(\boldsymbol{r},\sigma;\boldsymbol{r}',\sigma')|_{\boldsymbol{r}=\boldsymbol{r}'} \quad \text{(A4)}$$

for the time-even quantities and

$$\boldsymbol{s}_T(\boldsymbol{r}) = \sum_{\sigma,\sigma'} (\boldsymbol{\sigma})_{\sigma',\sigma}\;\rho_T(\boldsymbol{r},\sigma;\boldsymbol{r},\sigma'), \quad \text{(A5)}$$

$$\boldsymbol{T}_T(\boldsymbol{r}) = \sum_{\sigma,\sigma'} (\boldsymbol{\sigma})_{\sigma',\sigma}\,\nabla\cdot\nabla'\,\rho_T(\boldsymbol{r},\sigma;\boldsymbol{r}',\sigma')|_{\boldsymbol{r}=\boldsymbol{r}'}, \quad \text{(A6)}$$

$$\boldsymbol{j}_T(\boldsymbol{r}) = \frac{i}{2}\sum_\sigma (\nabla'-\nabla)\,\rho_T(\boldsymbol{r},\sigma;\boldsymbol{r}',\sigma)|_{\boldsymbol{r}=\boldsymbol{r}'} \quad \text{(A7)}$$

for the time-odd quantities. For the local densities $\tau_p(\boldsymbol{r})$, $\tau_n(\boldsymbol{r})$, and $\rho_p(\boldsymbol{r})$ in Eqs. (9) and (11) we have $\tau_p = (\tau_0-\tau_1)/2$, $\tau_n = (\tau_0+\tau_1)/2$, $\rho_p = (\rho_0-\rho_1)/2$.

APPENDIX B: PARAMETERS OF THE SKYRME EDF

The following equations establish the relation between the C constants in Eq. (12) and the parameters of the Skyrme force t_0, x_0, t_1, x_1, t_2, x_2, t_3, x_3, W_0, and x_W

$$
\begin{aligned}
C_0^{\rho} &= \tfrac{3}{8}t_0, & C_1^{\rho} &= -\tfrac{1}{4}t_0\left(\tfrac{1}{2}+x_0\right),\\
C_0^{\rho,\alpha} &= \tfrac{1}{16}t_3, & C_1^{\rho,\alpha} &= -\tfrac{1}{24}t_3\left(\tfrac{1}{2}+x_3\right),\\
C_0^{\Delta\rho} &= -\tfrac{9}{64}t_1+\tfrac{5}{64}t_2+\tfrac{1}{16}t_2x_2, & C_1^{\Delta\rho} &= \tfrac{1}{32}\left[3t_1\left(\tfrac{1}{2}+x_1\right)+t_2\left(\tfrac{1}{2}+x_2\right)\right],\\
C_0^{\tau} &= \tfrac{3}{16}t_1+\tfrac{5}{16}t_2+\tfrac{1}{4}t_2x_2, & C_1^{\tau} &= -\tfrac{1}{8}\left[t_1\left(\tfrac{1}{2}+x_1\right)-t_2\left(\tfrac{1}{2}+x_2\right)\right],\\
C_0^{J} &= \tfrac{1}{8}\left[t_1\left(\tfrac{1}{2}-x_1\right)-t_2\left(\tfrac{1}{2}+x_2\right)\right]\eta_J, & C_1^{J} &= \tfrac{1}{16}(t_1-t_2)\,\eta_J,\\
C_0^{\nabla J} &= -\tfrac{1}{4}(2+x_W)W_0, & C_1^{\nabla J} &= -\tfrac{1}{4}x_W W_0,\\
C_0^{s} &= \tfrac{1}{2}C_{\rm N}\,g-\tfrac{1}{4}t_0\left(\tfrac{1}{2}-x_0\right)\eta_s, & C_1^{s} &= \tfrac{1}{2}C_{\rm N}\,g'-\tfrac{1}{8}t_0\,\eta_s,\\
C_0^{s,\alpha} &= -\tfrac{1}{24}t_3\left(\tfrac{1}{2}-x_3\right)\eta_{s,\alpha}, & C_1^{s,\alpha} &= -\tfrac{1}{48}t_3\,\eta_{s,\alpha},\\
C_0^{\Delta s} &= \tfrac{1}{32}\left[3t_1\left(\tfrac{1}{2}-x_1\right)+t_2\left(\tfrac{1}{2}+x_2\right)\right]\eta_{\Delta s}, & C_1^{\Delta s} &= \tfrac{1}{64}(3t_1+t_2)\,\eta_{\Delta s}.
\end{aligned}
\tag{B1}
$$

The formulas for the spin-orbit constants $C_T^{\nabla J}$ imply the parametrization introduced in Refs. [43,62] in which the spin-orbit term of the interaction is treated in the Hartree approximation. The parameters W_0 and x_W are related with the constants b_4 and b'_4 of Ref. [43] by the formulas: $W_0 = 2b_4$, $x_W = b'_4/b_4$. The parameter $\eta_J = 1$ if the J^2 terms are included in the Skyrme EDF and $\eta_J = 0$ if not. In the standard parametrizations, the parameters x_W, η_s, $\eta_{s,\alpha}$, and $\eta_{\Delta s}$ are equal to 1, the parameters g and g' are equal to 0.

[1] M. Bender, P.-H. Heenen, and P.-G. Reinhard, Rev. Mod. Phys. **75**, 121 (2003).
[2] A. B. Migdal, *Theory of Finite Fermi Systems and Application to Atomic Nuclei* (Wiley, New York, 1967).
[3] P. Ring and J. Speth, Phys. Lett. B **44**, 477 (1973).
[4] I. N. Borzov, S. V. Tolokonnikov, and S. A. Fayans, Sov. J. Nucl. Phys. **40**, 732 (1984).
[5] J. Speth and J. Wambach, in *Electric and Magnetic Giant Resonances in Nuclei*, International Review of Nuclear Physics, Vol. 7, edited by J. Speth (World Scientific, Singapore, 1991), pp. 2–87.
[6] D. Vautherin and D. Brink, Phys. Rev. C **5**, 626 (1972).
[7] M. Beiner, H. Flocard, N. Van Giai, and P. Quentin, Nucl. Phys. A **238**, 29 (1975).
[8] J. Bartel, P. Quentin, M. Brack, C. Guet, and H.-B. Håkansson, Nucl. Phys. A **386**, 79 (1982).
[9] M. Brack, C. Guet, and H.-B. Håkansson, Phys. Rep. **123**, 275 (1985).
[10] P. Klüpfel, P.-G. Reinhard, T. J. Bürvenich, and J. A. Maruhn, Phys. Rev. C **79**, 034310 (2009).
[11] J. Speth, S. Krewald, F. Grümmer, P. G. Reinhard, N. Lyutorovich, and V. Tselyaev, Nucl. Phys. A **928**, 17 (2014).
[12] K. Wienhard, K. Ackermann, K. Bangert, U. E. P. Berg, C. Bläsing, W. Naatz, A. Ruckelshausen, D. Rück, R. K. M. Schneider, and R. Stock, Phys. Rev. Lett. **49**, 18 (1982).
[13] R. Köhler, J. A. Wartena, H. Weigmann, L. Mewissen, F. Poortmans, J. P. Theobald, and S. Raman, Phys. Rev. C **35**, 1646 (1987).
[14] R. M. Laszewski, R. Alarcon, D. S. Dale, and S. D. Hoblit, Phys. Rev. Lett. **61**, 1710 (1988).
[15] T. Shizuma, T. Hayakawa, H. Ohgaki, H. Toyokawa, T. Komatsubara, N. Kikuzawa, A. Tamii, and H. Nakada, Phys. Rev. C **78**, 061303(R) (2008).
[16] G. F. Bertsch, Nucl. Phys. A **354**, 157c (1981).
[17] J. D. Vergados, Phys. Lett. B **36**, 12 (1971).
[18] J. Speth, V. Klemt, J. Wambach, and G. E. Brown, Nucl. Phys. A **343**, 382 (1980).
[19] E. Migli, S. Drożdż, J. Speth, and J. Wambach, Z. Phys. A **340**, 111 (1991).
[20] L.-G. Cao, G. Colò, H. Sagawa, P. F. Bortignon, and L. Sciacchitano, Phys. Rev. C **80**, 064304 (2009).
[21] P. Vesely, J. Kvasil, V. O. Nesterenko, W. Kleinig, P.-G. Reinhard, and V. Y. Ponomarev, Phys. Rev. C **80**, 031302(R) (2009).
[22] V. O. Nesterenko, J. Kvasil, P. Vesely, W. Kleinig, P.-G. Reinhard, and V. Y. Ponomarev, J. Phys. G: Nucl. Part. Phys. **37**, 064034 (2010).
[23] L.-G. Cao, H. Sagawa, and G. Colò, Phys. Rev. C **83**, 034324 (2011).
[24] P. Wen, L.-G. Cao, J. Margueron, and H. Sagawa, Phys. Rev. C **89**, 044311 (2014).
[25] J. S. Dehesa, J. Speth, and A. Faessler, Phys. Rev. Lett. **38**, 208 (1977).
[26] S. P. Kamerdzhiev and V. N. Tkachev, Phys. Lett. B **142**, 225 (1984).
[27] D. Cha, B. Schwesinger, J. Wambach, and J. Speth, Nucl. Phys. A **430**, 321 (1984).
[28] D. T. Khoa, V. Y. Ponomarev, and A. I. Vdovin, Preprint JINR **E4-86-198** (1986).
[29] S. P. Kamerdzhiev and V. N. Tkachev, Z. Phys. A **334**, 19 (1989).
[30] V. I. Tselyaev, Sov. J. Nucl. Phys. **50**, 780 (1989).
[31] S. P. Kamerdzhiev, J. Speth, G. Tertychny, and J. Wambach, Z. Phys. A **346**, 253 (1993).
[32] V. Tselyaev, N. Lyutorovich, J. Speth, and P.-G. Reinhard, Phys. Rev. C **96**, 024312 (2017).

[33] V. Tselyaev, N. Lyutorovich, J. Speth, and P.-G. Reinhard, Phys. Rev. C **97**, 044308 (2018).
[34] J. S. Bell and T. H. R. Skyrme, Philos. Mag. **1**, 1055 (1956).
[35] T. H. R. Skyrme, Nucl. Phys. **9**, 635 (1959).
[36] J. Dobaczewski and J. Dudek, Phys. Rev. C **52**, 1827 (1995).
[37] J. Dobaczewski and J. Dudek, Acta Phys. Pol. B **27**, 45 (1996).
[38] Y. M. Engel, D. M. Brink, K. Goeke, S. J. Krieger, and D. Vautherin, Nucl. Phys. A **249**, 215 (1975).
[39] N. Van Giai and H. Sagawa, Phys. Lett. B **106**, 379 (1981).
[40] M. Rayet, M. Arnould, F. Tondeur, and G. Paulus, Astron. Astrophys. **116**, 183 (1982).
[41] F. Tondeur, M. Brack, M. Farine, and J. M. Pearson, Nucl. Phys. A **420**, 297 (1984).
[42] J. Dobaczewski, H. Flocard, and J. Treiner, Nucl. Phys. A **422**, 103 (1984).
[43] P.-G. Reinhard and H. Flocard, Nucl. Phys. A **584**, 467 (1995).
[44] E. Chabanat, P. Bonche, P. Haensel, J. Meyer, and R. Schaeffer, Nucl. Phys. A **635**, 231 (1998).
[45] B. A. Brown, Phys. Rev. C **58**, 220 (1998).
[46] P.-G. Reinhard, D. J. Dean, W. Nazarewicz, J. Dobaczewski, J. A. Maruhn, and M. R. Strayer, Phys. Rev. C **60**, 014316 (1999).
[47] F. Tondeur, S. Goriely, J. M. Pearson, and M. Onsi, Phys. Rev. C **62**, 024308 (2000).
[48] S. Goriely, M. Pearson, and F. Tondeur, Nucl. Phys. A **688**, 349c (2001).
[49] N. Lyutorovich, V. I. Tselyaev, J. Speth, S. Krewald, F. Grümmer, and P.-G. Reinhard, Phys. Rev. Lett. **109**, 092502 (2012).
[50] X. Roca-Maza, G. Colò, and H. Sagawa, Phys. Rev. C **86**, 031306(R) (2012).
[51] N. Lyutorovich, V. Tselyaev, J. Speth, S. Krewald, F. Grümmer, and P.-G. Reinhard, Phys. Lett. B **749**, 292 (2015).
[52] N. Lyutorovich, V. Tselyaev, J. Speth, S. Krewald, and P.-G. Reinhard, Phys. At. Nucl. **79**, 868 (2016).
[53] V. Tselyaev, N. Lyutorovich, J. Speth, S. Krewald, and P.-G. Reinhard, Phys. Rev. C **94**, 034306 (2016).
[54] S. Kamerdzhiev, J. Speth, and G. Tertychny, Phys. Rep. **393**, 1 (2004).
[55] I. Poltoratska, P. von Neumann-Cosel, A. Tamii, T. Adachi, C. A. Bertulani, J. Carter, M. Dozono, H. Fujita, K. Fujita, Y. Fujita, K. Hatanaka, M. Itoh, T. Kawabata, Y. Kalmykov, A. M. Krumbholz, E. Litvinova, H. Matsubara, K. Nakanishi, R. Neveling, H. Okamura, H. J. Ong, B. Özel-Tashenov, V. Y. Ponomarev, A. Richter, B. Rubio, H. Sakaguchi, Y. Sakemi, Y. Sasamoto, Y. Shimbara, Y. Shimizu, F. D. Smit, T. Suzuki, Y. Tameshige, J. Wambach, M. Yosoi, and J. Zenihiro, Phys. Rev. C **85**, 041304(R) (2012).
[56] J. Birkhan, H. Matsubara, P. von Neumann-Cosel, N. Pietralla, V. Y. Ponomarev, A. Richter, A. Tamii, and J. Wambach, Phys. Rev. C **93**, 041302(R) (2016).
[57] S. Stringari, R. Leonardi, and D. M. Brink, Nucl. Phys. A **269**, 87 (1976).
[58] M. Bender, J. Dobaczewski, J. Engel, and W. Nazarewicz, Phys. Rev. C **65**, 054322 (2002).
[59] N. Chamel, S. Goriely, and J. M. Pearson, Phys. Rev. C **80**, 065804 (2009).
[60] T. Lesinski, M. Bender, K. Bennaceur, T. Duguet, and J. Meyer, Phys. Rev. C **76**, 014312 (2007).
[61] A. Pastore, D. Tarpanov, D. Davesne, and J. Navarro, Phys. Rev. C **92**, 024305 (2015).
[62] M. M. Sharma, G. Lalazissis, J. König, and P. Ring, Phys. Rev. Lett. **74**, 3744 (1995).
[63] G. A. Lalazissis, D. Vretenar, W. Pöschl, and P. Ring, Phys. Lett. B **418**, 7 (1998).
[64] O. Moreno, E. Moya de Guerra, P. Sarriguren, and A. Faessler, Phys. Rev. C **81**, 041303(R) (2010).
[65] E. Moya de Guerra, O. Moreno, and P. Sarriguren, J. Phys.: Conf. Ser. **312**, 092045 (2011).
[66] M. Kortelainen, T. Lesinski, J. Moré, W. Nazarewicz, J. Sarich, N. Schunck, M. V. Stoitsov, and S. Wild, Phys. Rev. C **82**, 024313 (2010).
[67] J. Dobaczewski, W. Nazarewicz, and P.-G. Reinhard, J. Phys. G **41**, 074001 (2014).
[68] V. I. Tselyaev, N. A. Lyutorovich, and N. A. Belov, Bull. Russ. Acad. Sci. Phys. **75**, 899 (2011).
[69] S. Drożdż, S. Nishizaki, J. Speth, and J. Wambach, Phys. Rep. **197**, 1 (1990).